Since January 2020 Elsevier has created a COVID-19 resource centre with free information in English and Mandarin on the novel coronavirus COVID-19. The COVID-19 resource centre is hosted on Elsevier Connect, the company's public news and information website.

Science of the Total Environment 744 (2020) 140840

Contents lists available at ScienceDirect

Science of the Total Environment

journal homepage: www.elsevier.com/locate/scitotenv

Levels and sources of hourly $PM_{2.5}$-related elements during the control period of the COVID-19 pandemic at a rural site between Beijing and Tianjin

Yang Cui [a,b], Dongsheng Ji [a,b,c,*], Willy Maenhaut [d,**], Wenkang Gao [a], Renjian Zhang [e,f], Yuesi Wang [a,b,c]

[a] State Key Laboratory of Atmospheric Boundary Layer Physics and Atmospheric Chemistry, Institute of Atmospheric Physics, Chinese Academy of Sciences, Beijing, China
[b] University of Chinese Academy of Sciences, Beijing, China
[c] Center for Excellence in Regional Atmospheric Environment, Institute of Urban Environment, Chinese Academy of Science, Xiamen 361021, China
[d] Department of Chemistry, Ghent University, Gent 9000, Belgium
[e] Key Laboratory of Regional Climate-Environment Research for Temperate East Asia, Institute of Atmospheric Physics, Chinese Academy of Sciences, Beijing 100029, China
[f] Xianghe Observatory of Whole Atmosphere, Institute of Atmospheric Physics, Chinese Academy of Sciences, Xianghe County, Hebei Province 065400, China

HIGHLIGHTS

- The effects of COVID-19 and its control were studied for a rural site in Xianghe.
- $PM_{2.5}$-related elements were hourly measured during our study.
- Dust, coal combustion and industrial sources decreased during the control period.
- Beyond expectation, vehicle emissions increased during the control period.
- Lowest reductions of industrial emission occurred for air masses from northeast.

GRAPHICAL ABSTRACT

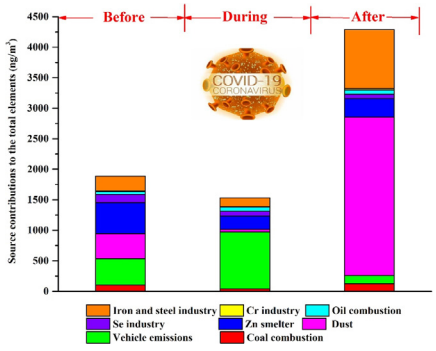

ARTICLE INFO

Article history:
Received 11 June 2020
Received in revised form 4 July 2020
Accepted 7 July 2020
Available online 9 July 2020

Keywords:
COVID-19
Emission reduction
Elements
$PM_{2.5}$
Xianghe
China

ABSTRACT

To control the spread of the novel coronavirus disease 2019 (COVID-19) in China, many anthropogenic activities were reduced and even closed on the national scale. To study the impact of this reduction and closing down, hourly concentrations of $PM_{2.5}$-related elements were measured at a rural site before (12–25 January 2020), during (26 January–9 February 2020) and after (22 March–2 April 2020) the control period when all people remained socially isolated in their homes and could not return to economic zones for work. Nine major sources were identified by the positive matrix factorization model, including fireworks burning, coal combustion, vehicle emissions, dust, Cr industry, oil combustion, Se industry, Zn smelter, and iron and steel industry. Before the control period, K, Fe, Ca, Zn, Ba and Cu were the main elements, and fireworks burning, Zn smelter and vehicle emissions provided the highest contributions to the total element mass with 55%, 12.1% and 10.3%, respectively. During the control period, K, Fe, Ba, Cu and Zn were the dominating elements, and fireworks burning and vehicle emissions contributed 55% and 27% of the total element mass. After the control period, Fe, K, Ca, Zn and Ba were the main elements, and dust and iron and steel industry were responsible for 56% and 21% of the total element mass. The increased contribution from vehicle emissions during the control period could be attributed to our sampling site being near a town hospital and the fact that the vehicle activities were not restricted. The source apportionment results were also related to air mass backward trajectories. The largest reductions of dust, coal

* Correspondence to: D. Ji, State Key Laboratory of Atmospheric Boundary Layer Physics and Atmospheric Chemistry, Institute of Atmospheric Physics, Chinese Academy of Sciences, Beijing, China.
** Corresponding author.
E-mail addresses: jds@mail.iap.ac.cn (D. Ji), Willy.Maenhaut@UGent.be (W. Maenhaut).

https://doi.org/10.1016/j.scitotenv.2020.140840

combustion, and the industrial sources (Cr industry, Zn smelter, Se industry, iron and steel industry) were distinctly seen for northwest transport (Ulanqab) and were least significant for northeast transport (Tangshan and Tianjin).

1. Introduction

The recent outbreak of the coronavirus disease 2019 (COVID-19) became a global pandemic impacting over 200 countries with over 7 million confirmed cases until 10 June 2020 (WHO, 2020). As the first country fighting COVID-19, China has implemented a series of control measures, including stay-at-home orders, closing non-essential businesses, and regional lockdown, etc. On 23 January 2020, the government of Wuhan announced a shutdown and other cities of Hubei announced a lockdown on 24 January 2020, which included actions such as quarantining, traffic restrictions, and factory closures. On 25 January 2020, all provinces in mainland China except Tibet launched the highest level of emergency response. Additionally, most provincial governments in China allowed non-essential businesses to resume work after 10 February (Zhang et al., 2020), while Wuhan began to cancel control measures and resume the production and common living order on 8 April (Hubei COVID-19 Headquarter, 2020).

During the control period of the pandemic, a series of measures was undertaken to reduce gatherings of people. Most transportation was prohibited and almost all avoidable outdoor anthropogenic activities stopped all around the country. The Spring Festival holiday was extended beyond 10 February, and only essential enterprises involving people's immediate needs (e.g., health care, providing food) were allowed to operate. All non-essential factories were shut down, and all schools, entertainment venues and restaurants were closed. This lockdown enforced restrictions and self-quarantine measures resulted in a dramatically reduced number of vehicles on the road and a near total reduction in factory production. The flow of commercial trucks and buses in the Beijing-Tianjin-Hebei region and its surrounding areas decreased by 77% and 39%, respectively, during the control period (Y. Wang et al., 2020). P. Wang et al. (2020) found that decreased anthropogenic emissions contributed to a decrease of $PM_{2.5}$ mass concentrations due to suspension of transportation and industry. The variations of air pollution during the control period provide an opportunity for better understanding the air quality improvement when significant restrictions in emissions from many sources are implemented.

To date, some studies have found that strict quarantine measures to control COVID-19 improved China's air quality in the short term (P. Wang et al., 2020; Y. Wang et al., 2020; Xu et al., 2020; Zhang et al., 2020). Compared with before the control period, the concentrations of NO_2, CO, $PM_{2.5}$, PM_{10} and SO_2 decreased during the control period, while the concentrations of O_3 increased. However, the variations and contributions of emission sources during this period are still rarely reported (Li et al., 2020; Zheng et al., 2020), in particular for rural areas. Trace elements can act as markers for specific source categories of $PM_{2.5}$ (Cui et al., 2019; Y. Liu et al., 2019). For example, arsenic (As) is used to indicate coal combustion, Cr is a tracer of industry (Cui et al., 2019). To study the variations of the $PM_{2.5}$ sources, hourly $PM_{2.5}$-related elements were measured at a rural site between Beijing and Tianjin in this study. The impact of regional transportation on $PM_{2.5}$ was analyzed by combining the backward trajectories with the results of source apportionment. This study provides useful information for other countries to assess the impact of COVID-19 on the environment and can be used as a reference for future research on improving air quality.

2. Methodology

2.1. Sampling site

The measurement period is from 12 January to 2 April 2020 at the Xianghe Atmospheric Integrated Observatory (39.75°N, 116.96°E) at a height of 8 m. Xianghe is a small county with 0.33 million residents, and it is located in a major plainlike area 50 km southeast of Beijing and 70 km north of Tianjin (Fig. 1). As shown in Fig. 1(b), a town hospital and a road are located at approximately 100 m to the northeast and east of the sampling site, respectively.

2.2. Instrumentation

The hourly $PM_{2.5}$ mass concentration was measured using a synchronized hybrid ambient real-time particulate monitor (model 5030,

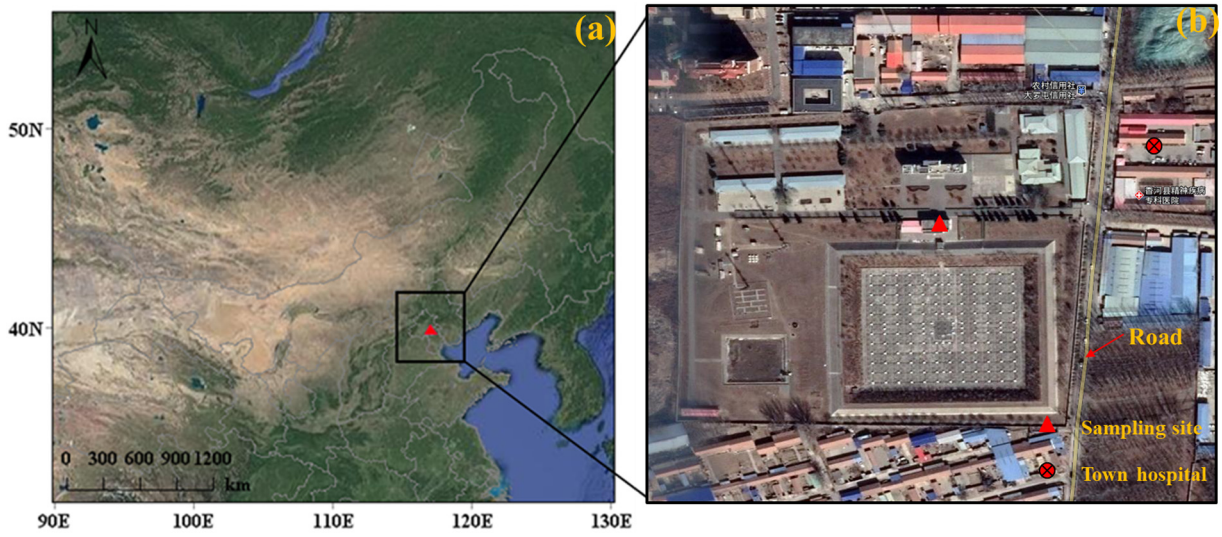

Fig. 1. Map of the sampling site in Xianghe (the red triangle and circle indicate the location of the sampling site and town hospital, respectively).

Thermo-Fisher, USA) in rural Xianghe. The hourly-mean $PM_{2.5}$ mass concentrations in "2 + 26" cities in Beijing-Tianjin-Hebei and its surrounding areas, including Beijing, Tianjin and seven cities (Jinan, Dezhou, Liaocheng, Bingzhou, Zibo, Jining, Heze) in the Shandong Province, eight cities (Langfang, Tangshan, Shijiazhuang, Handan, Baoding, Cangzhou, Hengshui, Xingtai) in the Hebei Province, four cities (Taiyuan, Changzhi, Jincheng, Yangquan) in the Shanxi Province and seven cities (Zhengzhou, Anyang, Kaifeng, Jiaozuo, Xinxing, Hebi and Puyang) in the Henan Province, were downloaded from the China National Environmental Monitoring Center (CNEMC) (available at http://106.37.208.233:20035/). The locations of the "2 + 26" cities and Xianghe are shown in Fig. S1. Elements in $PM_{2.5}$ were measured with 1-h time resolution by an Xact 625 Ambient Metals Monitor (Cooper Environmental Services (CES), Beaverton, OR, USA). This instrument is a sampling and analyzing X-ray fluoresce spectrometer designed for the semi-continuous measurement of elements in aerosols; it can measure 23 elements, i.e., K, Ca, V, Cr, Cu, Zn, Ga, As, Mn, Fe, Co, Ni, Se, Ag, Cd, Sn, Sb, Au, Hg, Ba, Tl, Pb, and Pd. More information on the instrument, as used by us, is given in Cui et al. (2019). For Co, Sn, Sb, and Tl, more than 85% of the data were below the method determination limit (MDL) and these elements were therefore excluded from the further analysis. More than 70% of the hourly concentrations of Ga, Ag, Cd and Au were below 3 × MDL and these were also excluded in this study. V was retained as it is an important tracer of oil combustion (Liu et al., 2018; Wang et al., 2018). The Xact 625 has already been used in several studies (Chang et al., 2018; Gao et al., 2016; Phillips-Smith et al., 2017; Tremper et al., 2018). Due to malfunction of the instrument, data from the period of 11 February to 21 March are not available. The details about quality assurance (QA)/quality control (QC) can be found in the Supporting information.

Additionally, the concentrations of SO_2 and NOx ($NOx = NO + NO_2$) were measured by a pulsed-fluorescence analyzer (model 43i, Thermo, USA) and a chemiluminescence analyzer (model 42i, Thermo, USA), respectively. Wind speed (*WS*) and wind direction (*WD*) were measured with an automatic weather station.

2.3. Positive matrix factorization (PMF) model for source apportionment

The PMF model is a widely used receptor model to resolve pollution sources and quantify the source contributions to the particulate matter (Gao et al., 2016; Wang et al., 2019; Zíková et al., 2016). The US EPA PMF5.0 model was employed to quantify the mass contributions and the source profiles of the elements in $PM_{2.5}$ in this study (Liu et al., 2018). The error fraction in the PMF analysis was set to 10% for the elements (Khan et al., 2016; Li et al., 2017). The detailed information about the calculation of the uncertainties of the measured elements can be found in the Supporting information. The uncertainties of the results from the PMF analysis were evaluated by displacement (DISP) and bootstrap (BS) (Paatero et al., 2014).

2.4. Air mass backward trajectory analysis

The 48-h backward trajectories arriving at the study site at a height of 500 m were calculated every hour using the Global Data Assimilation System meteorological data set (ftp://arlftp.arlhq.noaa.gov/pub/archives/gdas1). Cluster analysis was performed using the GIS-based software named TrajSat (Wang et al., 2009).

3. Results and discussion

3.1. Concentrations of $PM_{2.5}$ mass during the study period

The time-series of hourly $PM_{2.5}$ mass concentrations in Xianghe and Beijing, Tianjin, Tangshan and Langfang in Hebei province during the study period are shown in Fig. 2. The $PM_{2.5}$ mass shows a similar variation in Xianghe and Beijing, Tianjin, Langfang, and Tangshan, indicating that the pollution of $PM_{2.5}$ is regional (Table S1). The hourly $PM_{2.5}$ mass concentrations in Xianghe varied from 2.2 μg/m^3 to 450 μg/m^3, with an average value of 76 ± 80 μg/m^3. The average values of the $PM_{2.5}$ mass concentrations (μg/m^3) in Xianghe and "2 + 26" cities in Beijing-Tianjin-Hebei and its surrounding areas during the study period are given in Table 1. The average concentrations of the $PM_{2.5}$ mass in Xianghe are higher than in Beijing, Tianjin and most cities in the Hebei, Shanxi, Shandong and Henan provinces, while they are lower than in Shijiazhuang, Handan, Baoding, Xingtai in the Hebei province and in Anyang, Kaifeng and Puyang in the Henan province.

From 10 February 2020 on, except for Hubei, some industrial activities and businesses began to resume work in some provinces, including Beijing, Tianjin and Hebei. The news reported that the percentage of work resumption of large industrial enterprises in Beijing reached about 90% on 16 March 2020 (China News, 2020). According to governmental intervention, the daily transportation index provided by the Baidu migration dataset (Baiduqianxi, 2020) and conditions of resuming work of some industries and businesses in Beijing, Tianjin and Langfang, three periods were selected to better illustrate the source emission changes: before the control period of the pandemic (P1: 12–25 January 2020), during the control period of the pandemic (P2: 26 January–9 February 2020) and after the control period of the pandemic (P3: 22 March–2 April 2020). It is worth noting that the average

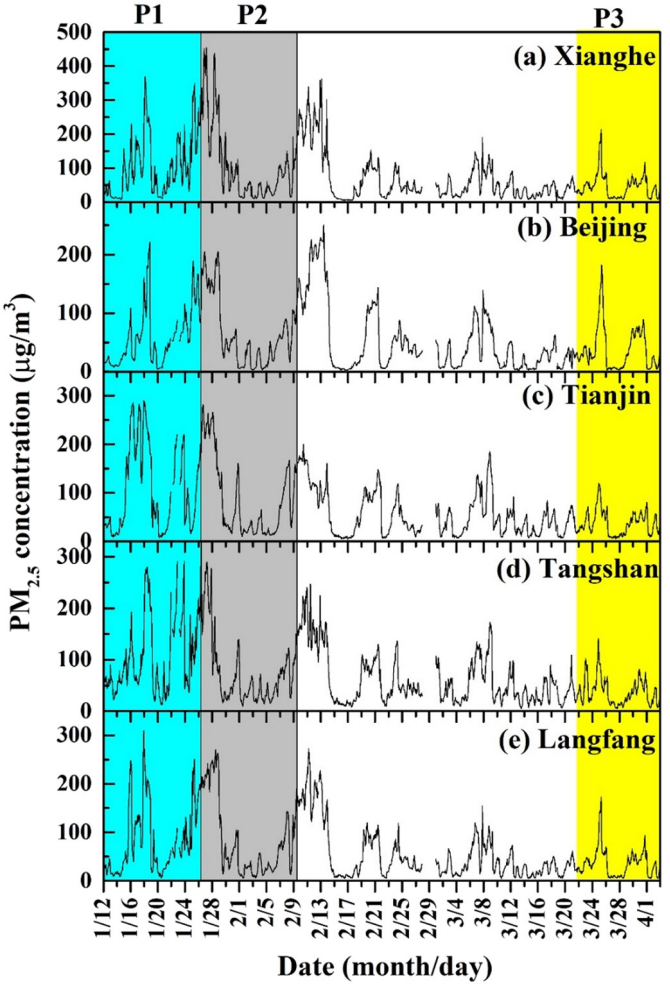

Fig. 2. Time series of the $PM_{2.5}$ mass in Xianghe (a), Beijing (b), Tianjin (c), Tangshan (d) and Langfang (e) during the intensive measurement period. The blue, gray and yellow shaded areas represent three periods: before the control period (P1), during the control period (P2) and after the control period (P3).

Table 1
Comparison of the average values of the $PM_{2.5}$ mass concentration (μg/m^3) in Xianghe and "2 + 26" cities in Beijing-Tianjin-Hebei and its surrounding areas during the entire measurement period (E) and the three control periods (P1, P2, and P3).

Cities	E	P1	P2	P3
Xianghe	76 ± 80	99 ± 84	114 ± 4	46 ± 35
Beijing	52 ± 53	57 ± 49	68 ± 110	38 ± 37
Tianjin	67 ± 64	106 ± 89	90 ± 58	38 ± 25
Langfang	61 ± 62	79 ± 69	89 ± 84	36 ± 29
Tangshan	67 ± 59	101 ± 70	82 ± 60	38 ± 26
Shijiazhuang	83 ± 65	145 ± 71	114 ± 80	52 ± 33
Baoding	81 ± 80	138 ± 113	121 ± 55	40 ± 23
Handan	78 ± 59	151 ± 63	103 ± 71	40 ± 17
Cangzhou	65 ± 56	119 ± 773	82 ± 79	35 ± 18
Hengshui	67 ± 51	130 ± 60	80 ± 57	37 ± 18
Xingtai	78 ± 59	146 ± 62	99 ± 48	45 ± 22
Taiyuan	68 ± 53	119 ± 72	83 ± 52	55 ± 38
Changzhi	58 ± 43	120 ± 52	66 ± 47	40 ± 21
Jincheng	62 ± 52	129 ± 75	70 ± 28	48 ± 26
Yangquan	59 ± 43	87 ± 48	70 ± 32	60 ± 39
Jinan	62 ± 41	111 ± 47	77 ± 36	38 ± 20
Dezhou	68 ± 59	147 ± 47	81 ± 34	34 ± 20
Liaocheng	71 ± 52	142 ± 68	87 ± 49	40 ± 20
Binzhou	59 ± 46	95 ± 60	69 ± 51	41 ± 26
Zibo	64. ± 41	100 ± 49	76 ± 47	49 ± 29
Jining	72 ± 45	125 ± 41	85 ± 37	44 ± 20
Heze	69 ± 49	139 ± 43	90 ± 50	37 ± 17
Zhengzhou	70 ± 50	130 ± 67	86 ± 47	41 ± 19
Anyang	90 ± 72	180 ± 85	112 ± 30	46 ± 22
Kaifeng	77 ± 56	147 ± 73	100 ± 60	39. ± 19
Jiaozuo	72 ± 48	131 ± 63	84 ± 43	50 ± 20
Xinxiang	64 ± 44	118 ± 60	74 ± 27	40. ± 17
Hebi	76 ± 55	143 ± 72	90 ± 28	45 ± 17
Puyang	80 ± 56	150 ± 51	102 ± 43	42 ± 20

$PM_{2.5}$ mass concentration in Xianghe was higher during P2 than during P1, which is similar to the variations in Langfang and Beijing (Table 1). In contrast, for all other cities of Table 1 the concentration of the $PM_{2.5}$ mass was lower during P2 than during P1. The different variations of the $PM_{2.5}$ mass concentrations during P1 and P2 can be attributed to meteorological conditions and increased secondary formation (Huang et al., 2020; P. Wang et al., 2020).

3.2. Element characteristics of the three selected periods

3.2.1. P1 before the control period

The time series of the concentrations of the hourly elements in $PM_{2.5}$ during the study period is shown in Fig. 3. K, Cu, Ba and Pb exhibited higher concentrations during the period from 24 January, 18:00 to 25 January, 12:00. 24 January is the Chinese New Year Eve, intensive fireworks burning during the Spring Festival (24 January–9 February 2020) have great effects on the concentrations of K, Cu, Ba and Pb, especially on the three nights of Chinese New year eve, Lunar Fifth Day, and the Lantern Festival. Major oxidizers in the fireworks are potassium compounds such as KNO_3, $KClO_3$, $KClO_4$, K_2CrO_4, and $K_2Cr_2O_7$ (Azhagurajan et al., 2011). Ba compounds are commonly used to generate green flames and are widely used as coloring agent and stabilizer (Zhang et al., 2017). Cu can generate blue flames and is used as a catalyzer (Kong et al., 2015). Pb as an oxidant (Pb_3O_4) can help to achieve a steady and reproducible burning rate (Kong et al., 2015; J. Liu et al., 2019). Other elements showed a different variation; Mn, Fe, Zn, As, Se exhibited slightly higher concentrations during the period of 15 to 19 January, which was related with higher contributions from different industries. Except for the effects of fireworks burning, some industries also affected the concentrations of Pb; Pb also showed higher concentrations during the period of 15 to 19 January. Cu also presented a higher concentration during the non-firework burning period; this could be attributed to the effects from vehicle emissions during travel before the Spring Festival (Zhu et al., 2018).

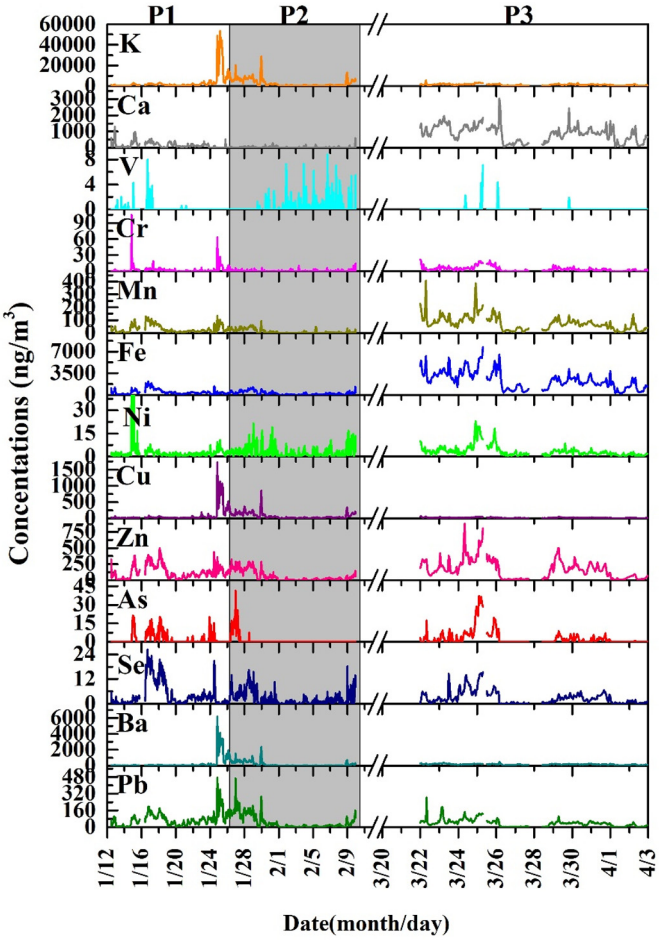

Fig. 3. Time series of the concentrations of the elements in $PM_{2.5}$ in Xianghe during the three periods (P1, P2 and P3). The shaded area represents the period (P2) during the control period of the COVID-19 pandemic.

3.2.2. P2 during the control period

During P2, K, Cu, Ba, and Pb still exhibited higher concentrations during the period of 26 to 29 January 2020 (Fig. 3). This could reflect aging processes after the emission of fireworks burning on the Chinese New Year Eve night (Kong et al., 2015). The occurrences of peak values of K, Cu, Ba and Pb on 29 January, 23:00 and 8 February, 22:00 were caused by fireworks burning, which occurred on the Lunar Fifth Day and the Lantern Festival, respectively. From 30 January 2020 on, almost all elements, with the exception of V and Ni, showed a very lower concentration, indicating that the control measures during the control period of the pandemic were effective. Table 2 gives the average concentrations and associated standard deviations for the various elements during the three periods. Compared with P1, the concentrations of Ca, Cr, Mn, Fe, Zn, As and Se also decreased during P2, which could be caused by the control measures conducted for fighting COVID-19, including social distancing, stay-at-home orders, closing non-essential businesses, and regional lockdown. 10 February 2020 was the first day of resuming work for many provinces, including Beijing, Tianjin and Hebei; as a result, the concentrations of some elements like Cu, Cr, Zn and Pb began to increase.

3.2.3. P3 after the control period

During P3, many industrial activities and businesses already resumed work. The percentage of work resumption of large industrial enterprises in the Hebei province reached 92% on 1 March 2020 (Hebei News, 2020); the percentage of work resumption of large industrial enterprises in Beijing reached about 90% on 16 March 2020 (China News,

Table 2
Average concentrations (ng/m^3) and associated standard deviations of elements in $PM_{2.5}$ at our study site during the three selected periods.

Element	P1	P2	P3
K	3400 ± 8100	3100 ± 4200	1310 ± 710
Ca	164 ± 174	23 ± 51	870 ± 500
V	0.2 ± 0.7	0.5 ± 1.7	0.1 ± 0.6
Cr	2.8 ± 8.0	1.0 ± 2.1	4.0 ± 4.4
Mn	32 ± 30	12.4 ± 17.4	76 ± 57
Fe	460 ± 400	260 ± 280	2400 ± 1450
Ni	2.7 ± 6.3	3.2 ± 3.6	3.5 ± 3.5
Cu	81 ± 200	81 ± 109	21 ± 11
Zn	125 ± 105	68 ± 87	166 ± 150
As	2.5 ± 5.0	1.2 ± 5.0	3.1 ± 6.4
Se	4.4 ± 5.9	2.5 ± 3.3	2.8 ± 3.2
Ba	240 ± 740	210 ± 410	152 ± 70
Pb	71 ± 65	52 ± 71	39 ± 36

2020). On 2 May 2020, the percentage of work resumption of large industrial enterprises and construction sites in Beijing reached about 100%. As seen in Fig. 3, almost all elements showed higher concentrations during P3. Compared to P2, the concentrations of Ca, Cr, Mn, Ni, Zn, As and Se also increased during P3 (Table 2), which indicated that the work resumed to some degree. To further assess the contributions from different sources and exclude the effects of fireworks burning, source apportionment of the $PM_{2.5}$ elements was conducted; this will be provided in Section 3.3.

The concentrations of the elements during the three periods (P1, P2 and P3) in 2020 were also compared with those during the same periods in 2019 (Figs. S2, S3 and S4). The three periods (P1, P2 and P3) in 2019 were defined according to the days from the first day of the Chinese Spring Festival holiday. 4 February was the first day of the Chinese Spring Festival holiday in 2019. Thus, the corresponding P1, P2 and P3 periods in 2019 were 23 January to 5 February 2019, 6 to 10 February 2019, and 3 to 14 April 2019, respectively. Because the Chinese Spring Festival holiday in 2020 included the Lantern Festival, the fireworks burning on the Lantern Festival gave rise to substantially larger concentrations of K, Cu, Ba and Pb during P2 in 2020 when compared with 2019. The weakened supervision measures for dust and the large scale resumption of work at construction sites during P3 after the pandemic in 2020 is likely the reason why the concentrations of some crustal elements (e.g., Ca, Fe and Ba) are much larger than during the same period in 2019.

3.3. Sources of elements in $PM_{2.5}$

In this study, 13 of the measured elements were used for the PMF analysis. The whole dataset including P1, P2 and P3 was used for the PMF runs. We also ran the PMF model separately for each of the three periods and compared the results with those for the whole dataset. Solutions with from five to eleven factors solutions were examined for the whole dataset; the 9-factor solution provided the most reasonable source profiles. The detailed comparison and analysis is given in the Supporting information. The relations between the predicted and measured concentrations of the elements are given in Table S2. With the exception of V, the coefficients of determination (r^2-values) between the measured and predicted concentrations of the species for the 9-factor PMF solution are all higher than 0.90. The uncertainties of the PMF results for the 9-factor solution were evaluated by DISP and BS. There were no swaps in the DISP runs and more than 98% of the BS runs could be mapped to base runs, indicating that the PMF analysis results were stable and reliable. The nine factors were fireworks burning, coal combustion, vehicle emissions, Se industry, Cr industry, Zn smelter, oil combustion, dust, and iron and steel industry. Fig. 4 presents the source profiles identified by the PMF model, while the time series of the nine factors for the measurement period are shown in Fig. S5. The polar plots and diurnal variations of the pollution source concentrations (ng/m^3) during the study period are shown in Figs. 5 and 6, respectively. The average concentrations and contributions of the nine sources during the three periods are given in Table 3.

Factor 1 was identified as fireworks burning, because it has high loadings of K, Cu, Ba and Pb and these elements are reliable tracers of fireworks burning (Kong et al., 2015; J. Liu et al., 2019). The time series of this factor also showed three main peaks during the Chinese New Year Eve, the lunar fifth day and the Lantern Festival, respectively (Fig. S5). As seen in Fig. 5, the higher contribution of this factor occurred with *WS* less than 1 m/s and fireworks burning was a local source. The fireworks burning showed higher concentrations during the nighttime (20:00–5:00), which was consistent with the occurrence of the fireworks burning (Fig. 6). This factor contributed overall 40% of the total element mass in $PM_{2.5}$. During P1 and P2, fireworks burning was responsible for 55% of the total elements mass.

Factor 2 was considered as coal combustion; in this factor, arsenic (As) has the higher loading. As is reliable tracer of coal combustion (Cui et al., 2019). This factor contributed overall 2.1% of the total element mass. Although the concentration of SO_2 is also affected by the fireworks burning (Huang et al., 2012), coal combustion was somewhat positively correlated with SO_2 ($r^2 = 0.14$). As shown in Fig. 5, higher concentrations of coal combustion occurred with *WS* less than 2 m/s and higher than 4 m/s, indicating that both local emissions and regional transport both played a role. The concentrations of coal combustion during the pre-control period, control and post-control periods were 104 ng/m^3, 40 ng/m^3 and 123 ng/m^3, respectively (Table 3). The Kruskal-Wallis ANOVA test showed that there are significant differences for coal combustion during the three periods (Kruskal-Wallis chi-squared = 57, df = 2, p-value < 0.05). With the implementation of the project "Coal to Gas" in Xianghe, coal combustion is mainly used for industry (Zhao et al., 2020). The lower concentration of coal combustion during the control period indicates that the control of coal combustion was effective.

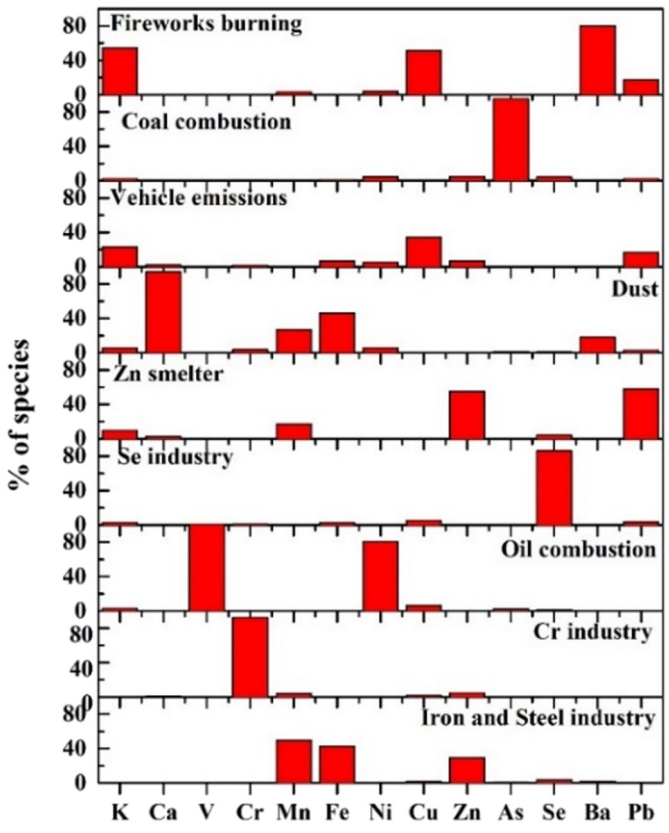

Fig. 4. Source profiles for the nine sources identified using the PMF model.

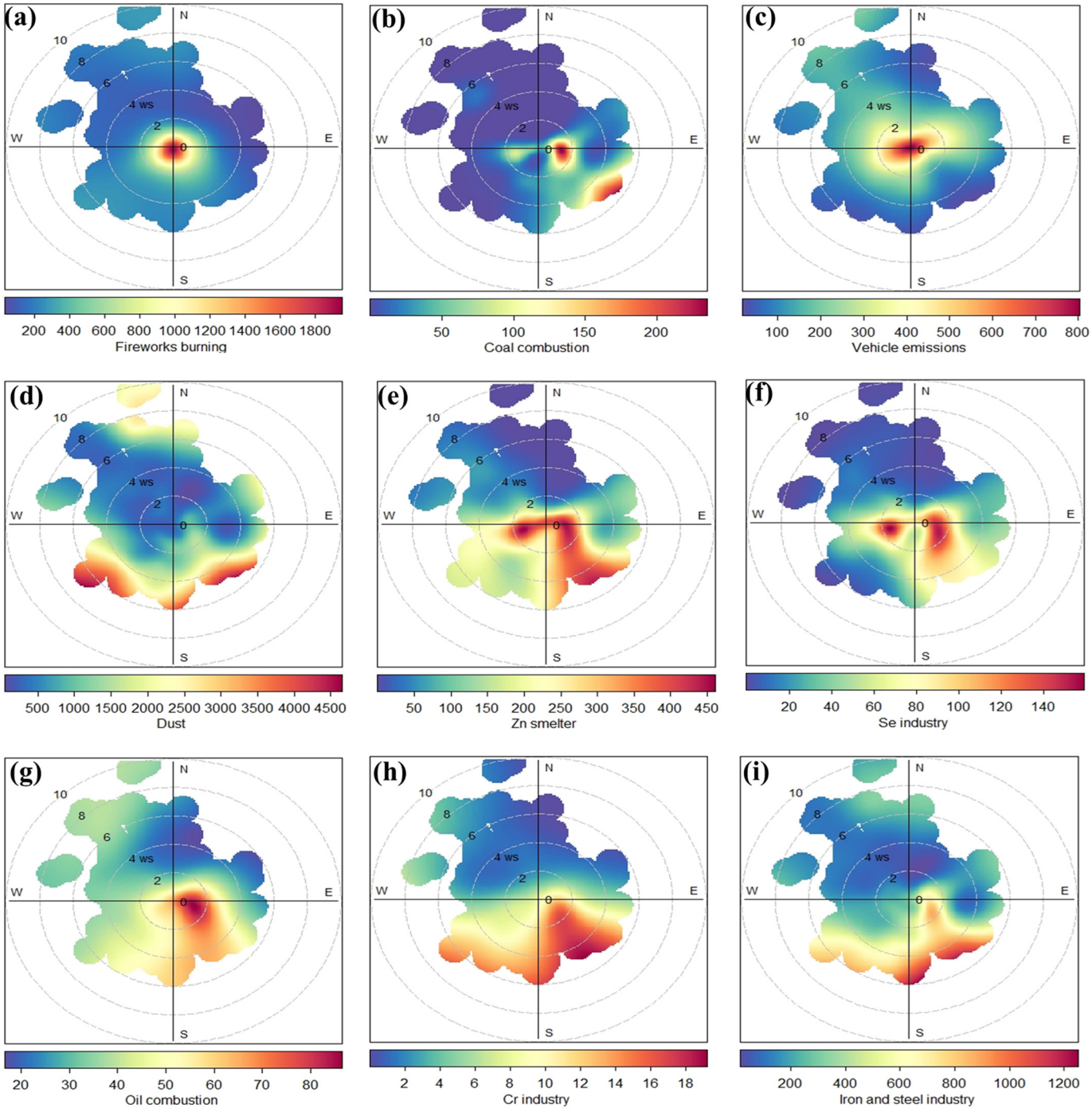

Fig. 5. Polar plots of pollution source concentrations (ng/m^3) during the study period in Xianghe (a: fireworks burning, b: coal combustion, c: vehicle emissions, d: dust, e: Zn smelter, f: Se industry, g: oil combustion, h: Cr industry, i: iron and steel industry). The dashed circles indicate the wind speed in m/s.

Factor 3 was linked to vehicle emissions, and it was characterized by high loadings of Cu (34%) and Zn (6.5%). According to the emission inventories of trace elements by Zhu et al. (2018), more than 55% of the Cu and about 10% of the Zn emissions originate from brake and tire wear. Cu is mainly used in lubricants and in friction materials that constitute major contents of brake linings, while Zn is added to the tire tread to facilitate the vulcanization process (Lin et al., 2015). The concentrations of NOx are also affected by the combustion of natural gas for heating in Xianghe (Zhao et al., 2020) in addition to the contribution from vehicle emissions; a moderate correlation between vehicle emissions and NOx was found ($r^2 = 0.40$). As shown in Fig. 5(c), the high contributions of vehicle emissions occurred with wind speeds of approximately 1 m/s. Thus, vehicle emissions were significantly affected by local emissions. Traffic activities on the road near the sampling site (approximately 100 m) were the main source of vehicle emissions. The diurnal variation for vehicle emissions (Fig. 6) shows morning and evening peaks and confirms the reasonability of this source identification. This factor contributed 13.3% of the total element mass during the measurement period. Across the pre-control period, the control period, and the post-control period, the mean concentrations from vehicle emissions were 430 ng/m^3, 930 ng/m^3 and 134 ng/m^3, respectively (Kruskal-Wallis chi-squared = 360, df = 2, p-value < 0.05). On 25 January 2020, all provinces except Tibet launched the highest level of emergency responses. In Xianghe, the government also implemented

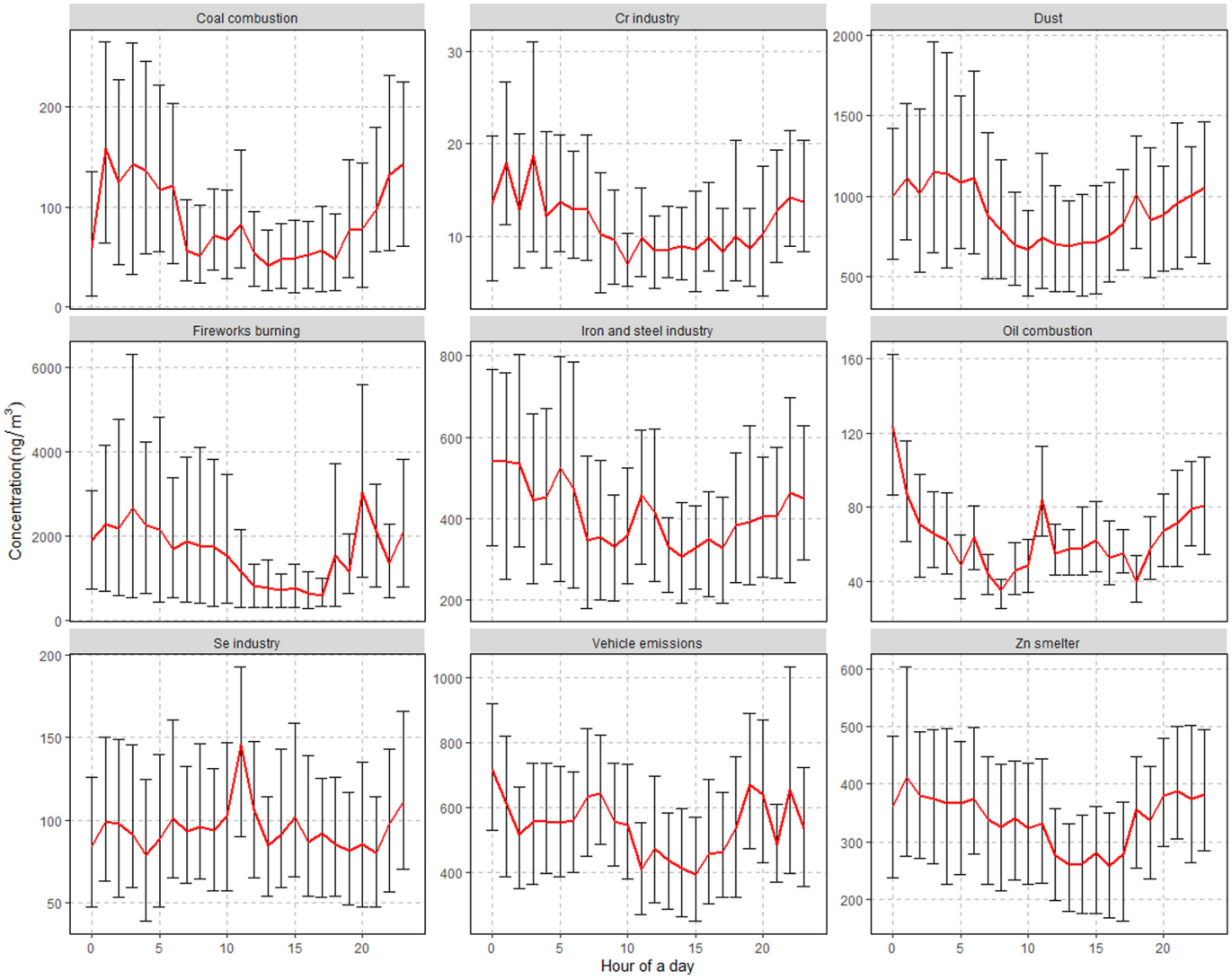

Fig. 6. Diurnal variations of the nine sources identified by the PMF model during the study period. The error bars represent the 95% confidence intervals of the mean (red lines).

a series to control the spread of the disease on 25 January 2020. Surprisingly, the concentrations of vehicle emissions did not decrease like was the case in Beijing and Tianjin according to the transportation index (Baiduqianxi, 2020). Possible reasons for this are: (1) our sampling site was located in a rural area in Xianghe, the vehicle emissions were not restricted strictly in the rural areas; thus, vehicle emissions still had higher contributions from 26 to 28 January 2020 (Fig. S5). From 28 January 2020 on, vehicle emissions showed decreased levels and exhibited lower concentrations during the period of 1 to 8 February 2020. On 9 February 2020, the increased vehicle emissions could be ascribed to some people going back to the city for work. The traffic flow within and between cities increased significantly with the resumption of work and production (MEP, 2020). (2) A town hospital is located at approximately 100 m to the east of our sampling site; the roads to the hospital were not restricted during the control period of COVID-2019. After the control period, lower contributions of vehicle emissions were observed due to the end of the Spring travel rush and relief of the pandemic; this then reflected the general condition of traffic flow on normal days near the sampling site. The road near the sampling site is not the main road in Xianghe and the traffic flow was not heavy.

Table 3
Average concentrations (*C*, ng/m^3) and contributions (%) of nine sources, as deduced by PMF for our study site, during the three periods.

Sources		P1	P2	P3	Average
Fireworks burning	*C*	2300	1890	360	1600
	%	55	55	7.7	40
Coal combustion	*C*	104	40	123	85
	%	2.5	1.2	2.6	2.1
Vehicle emissions	*C*	430	930	134	540
	%	10.3	27	2.9	13.3
Dust	*C*	410	45	2600	890
	%	9.8	1.4	56	22
Zn smelter	*C*	510	220	300	340
	%	12.1	6.5	6.4	8.4
Se industry	*C*	135	77	71	95
	%	3.2	2.3	1.5	2.3
Oil combustion	*C*	47	71	72	63
	%	1.1	2.1	1.5	1.5
Cr industry	*C*	12.0	4.5	19.9	11.3
	%	0.3	0.2	0.4	0.3
Iron and steel industry	*C*	240	147	970	410
	%	5.7	4.3	21	10.1

Factor 4 was identified as dust because it has high loading of Ca, Fe and Ba (Gao et al., 2016). Higher concentrations of dust came from the southern and northwestern areas of the sampling site with *WS* higher than 4 m/s. The average concentrations of dust during P1, P2 and P3 were 410 ng/m^3, 45 ng/m^3 and 2600 ng/m^3, respectively (Kruskal-

Wallis chi-squared = 660, df = 2, p-value < 0.05). The low dust concentration during P2 can be ascribed to the stop of construction activities, while the higher concentrations of dust during P3 were caused by higher dust in spring and the resumption of some construction sites.

Factor 5 was considered as a Zn smelter. In this factor, Zn and Pb showed a high loading. Mn also contributed somewhat. These metals were previously attributed to emissions from smelters (Dall'Osto et al., 2013). Amato et al. (2010) also reported a PMF factor with high concentrations of Zn, Pb and Mn and attributed it to industrial emissions, whereas a similar factor was attributed more to local workshops and ateliers in the city of Zurich (Richard et al., 2011). Higher concentrations of this factor were found for both low and high *WS*, thus both local and regional transportation contributed to it. Across the three periods, the source contributions were 510 ng/m^3, 220 ng/m^3 and 300 ng/m^3, respectively (Kruskal-Wallis chi-squared = 157, df = 2, p-value < 0.05).

Factor 6 was identified as Se industry. According to the emission inventory of the Se in the Beijing-Tianjin-Hebei region in 2012, nonmetallic mineral manufacturing accounts for 52% of the Se emission (Zhu et al., 2018). Glass production contributes the largest fraction of the Se emission (about 51%) because of the widespread application of selenium powder as decolorizing agent in the glass production process (Zhu et al., 2018). Hebei province is the largest producer of plate glass in China, accounting for about 19.9% of the national output (Zhu et al., 2018). As shown in Fig. 5, higher concentrations of this factor occurred with *WS* at 1–4 m/s for winds from western and southeastern areas of the sampling site. The contributions of the Se industry during the three periods (pre-control, control, post-control) were 135 ng/m^3, 77 ng/m^3, and 71 ng/m^3, respectively (Kruskal-Wallis chi-squared = 17.5, df = 2, p-value < 0.05).

Factor 7 has high loadings of V and Ni. These two elements are good indicators of oil combustion sources and thus this factor was identified as oil combustion. V and Ni are abundant in crude oil and primarily retained in fuel oil-related industrial products (i.e., marine heavy oil, industrial heavy oil, asphalt, and petroleum coke) during the oil refinery process (Liu et al., 2018). Heavy oil and petroleum coke are widely used as power fuels in petrochemical plants, marine heavy oil, small power plants, and construction industries. The concentrations of oil combustion during P1, P2 and P3 are 47 ng/m^3, 71 ng/m^3, and 72 ng/m^3, respectively (Kruskal-Wallis chi-squared = 15.6, df = 2, p-value < 0.05).

Factor 8 was identified as Cr-related industry emissions, with a high loading of Cr (92%). Cr is widely used in electroplating (additive metal surface treatment) and leather (as a chrome tanning agent used in the tanning process) industries (Liu et al., 2018). Specific metal processing industries have also been reported to be associated with Cr emissions (Querol et al., 2007). The higher concentrations of the Cr industry originated from the southeastern areas of the sampling site with *WS* at 1–6 m/s (Fig. 5). The concentrations of Cr industry during the pre-control period (P1), control (P2) and post-control periods (P3) were 12.0 ng/m^3, 4.5 ng/m^3 and 19.9 ng/m^3, respectively (Kruskal-Wallis chi-squared = 127, df = 2, p-value < 0.05).

Factor 9 was identified as iron and steel industry because of high loadings for Mn, Fe and Zn. Iron and steel production are among the most important industries in the Beijing-Tianjin-Hebei region (National Bureau of Statistics, 2017). The sintering process in iron and steel industries produces large amounts of heavy metals: Zn, Mn and Fe (Duan and Tan, 2013). According to the polar plot of this factor (Fig. 5), higher concentrations occurred for winds from the southeastern area of the sampling site with *WS* higher than 4 m/s. There are a lot of iron and steel plants in southeastern areas of the sampling site, like Tianjin and Tangshan (Zhu et al., 2018). The concentrations of iron and steel industry during the pre-control period, control and post-control periods were 240 ng/m^3, 147 ng/m^3 and 970 ng/m^3, respectively (Table 3) (Kruskal-Wallis chi-squared = 360, df = 2, p-value < 0.05).

As can be deduced from the concentration data in Table 3, compared with P1, the dust concentration during P2 decreased by 89%, followed by decreases for the Cr industry (62%), coal combustion (62%), Zn smelter (58%), Se industry (43%) and iron and steel industry (40%). In contrast, the concentrations from vehicle emissions and oil combustion increased by 115% and 53%, respectively.

3.4. Air mass backward trajectories during the three periods

During the study period (P1, P2 and P3), the air masses were classified into five clusters (Fig. 7(a)). Source contributions (ng/m^3) of eight factors for each trajectory cluster during the three periods (P1, P2 and P3) are also shown in Fig. 7(b). The air masses for Cluster 1 (C1) originated in Mongolia, passed over Xilingele League in Inner Mongolia, Chengde in Hebei; this cluster made up for 26.5% of the air masses. The air masses for Clusters 2 (C2) and 4 (C4) came from northwest areas of the sampling site; these clusters accounted for 16.7% and 24.6%, respectively, of the air masses. The transport distance was longer for C2 than for C4; the air masses for C2 originated from Siberia, while those for C4 started from Mongolia; the air masses of both clusters passed Ulanqab in Inner Mongolia and Zhangjiakou in the Hebei province before reaching Beijing. For Cluster 3 (C3), before reaching Beijing, the air masses passed Chengde and Tangshan in the Hebei province, and Tianjin. Tangshan and Tianjin are industrial cities in China. The contributions from coal combustion, Cr industry, Se industry, Zn smelter as well as from iron and steel industry were relatively larger for C3 than for the other clusters (Fig. 7(b)). The air masses for Cluster 5 (C5) came from southwestern areas of the sampling site; they successively passed Suqian and Xuzhou in the Jiangsu province, Jining and Liaocheng in the Shandong province, and Hengshui in the Hebei province. The passed areas of C5 are characterized by higher emissions from industrial activities (Zhu et al., 2018). It is worth noting that C5 only occurred during P3 after the control period (22 March–2 April 2020); its air mass trajectories accounted for 8.7% of all trajectories. During P3, in addition to C3, C5 also had higher contributions from industrial activities, which is consistent with air mass transport from the industrial regions in the southwestern Hebei province.

We examined the difference of contributions of eight sources during the three periods (P1, P2 and P3) for different clusters. Compared to P1, coal combustion showed almost 100% decrease for C1, C2 and C4 during P2, while the concentration of coal combustion for C3 only decreased by 24.9%. The lower reduction of coal combustion for C3 could be ascribed to no shutdown of some coal combustion related industries; note that lower reductions of some industrial sources were also observed for C3. Due to the stop of many construction activities during P2, the contributions of dust decreased by 86%, 79%, 94% and 92% for C1, C2, C3 and C4, respectively. Other industrial activities also showed a decrease during P2. The contributions of the Zn smelter decreased by 81%, 84%, 22% and 95% for C1, C2, C3 and C4, respectively. The Cr industry contributions decreased by 47%, 41%, 65% and 77% for C1, C2, C3 and C4, respectively. The contributions from the Se industry decreased by 55%, 47%, 41% and 64% for C1, C2, C3 and C4, respectively. The iron and steel industry contributions decreased by 71%, 34%, 19.1% and 87% for C1, C2, C3 and C4, respectively. In contrast to the concentrations from the dust, coal combustion and industrial sources, the concentrations of oil combustion and vehicle emissions increased during P2. The concentrations of oil combustion increased by 44%, 85%, 45% and 34% for C1, C2, C3 and C4 during P2 when compared with P1. Although the concentrations of vehicle emissions increased in all the clusters during the control period, they were mainly affected by local emissions; the reasons were discussed in Section 3.2. The least decreased contributions of coal combustion and industrial activities (Zn smelter, Se industry, iron and steel industry) during P2 were noted for C3 when the air masses passed over Tangshan and Tianjin.

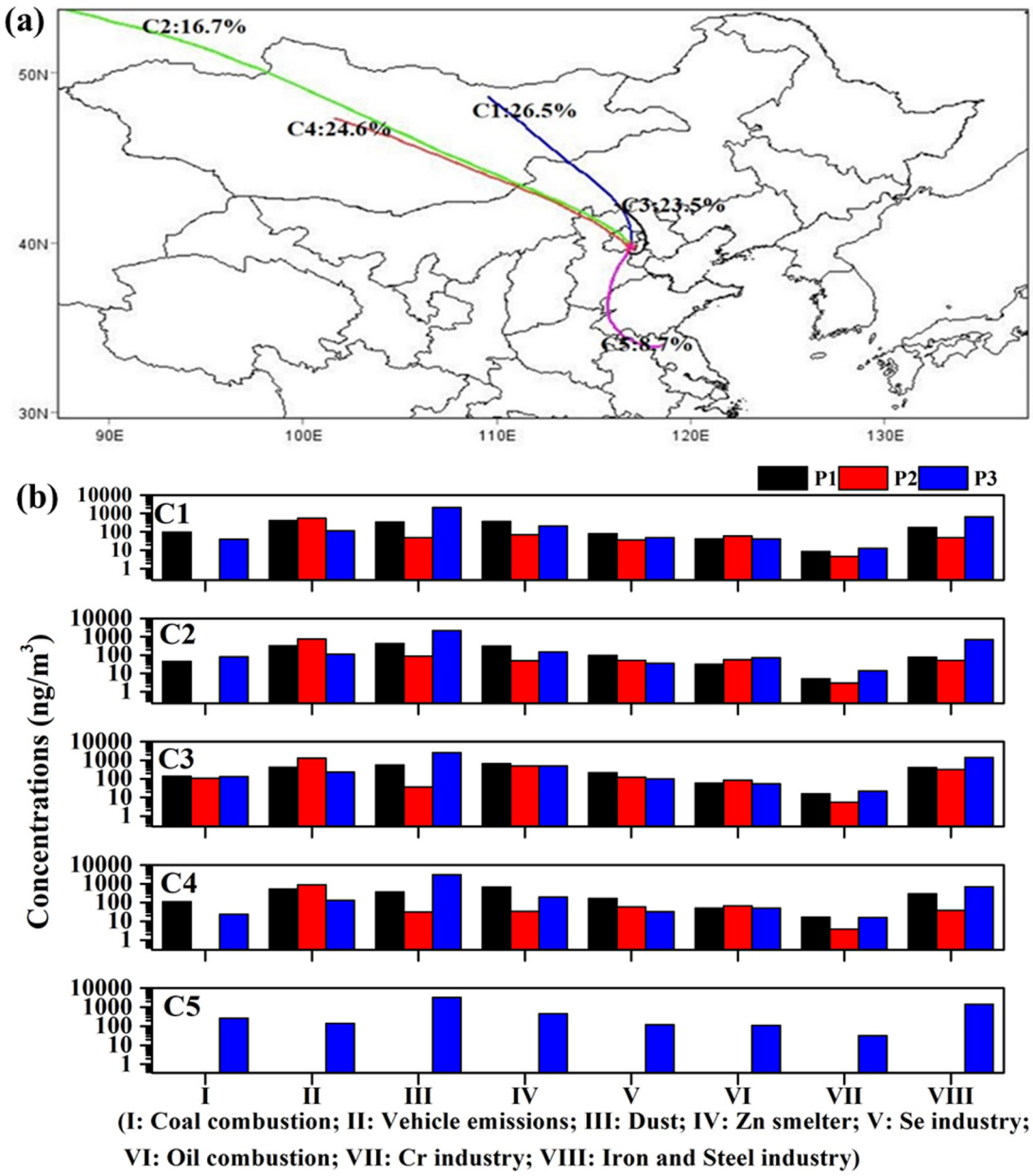

Fig. 7. Cluster analysis (a) of 48-h air mass back-trajectories arriving at Xianghe and concentrations (b) of each source from different air mass clusters for the study period including P1, P2 and P3.

Compared with P2, the concentrations of coal combustion in the different air mass clusters were higher during P3 after the control period, indicating the resumption of some coal combustion related industrial activities. However, as shown in Fig. 7(b), the concentrations of coal combustion during P3 in C1, C3 and C4 were lower than those before the control period. This is reasonable due to the stop of heating activities from 15 March 2020 on. Higher contributions of dust during P3 in all clusters can be ascribed to frequent occurrence of sand storms in spring and the resumption of large construction activities. The contributions of industrial sources (Cr industry, Se industry, Zn smelter, iron and steel industry) in different air masses during P3 were slightly higher than during P2, which also reflects the resumption of those industrial activities. The concentrations of some industrial sources like Zn smelter in different clusters were still lower during P3 than those during P1, which indicated that these industrial enterprises did not work yet at their normal operational levels. Vehicle emissions were lower during P3 when compared with those during P1 and P2; this is ascribed to the end of Spring travel rush and the relief of the pandemic.

4. Conclusion

Hourly concentrations of $PM_{2.5}$ mass and $PM_{2.5}$ related elements were measured from 12 January to 2 April 2020 at a rural site in Xianghe between Beijing and Tianjin. The following conclusions can be drawn:

(1) The average concentrations of the $PM_{2.5}$ mass during the study period in Xianghe were higher than those in most "2 + 26" cities in Beijing-Tianjin-Hebei and its surrounding areas. Similar to Beijing and Langfang, the $PM_{2.5}$ mass concentrations were higher during the control period when compared with before the control period.
(2) During the three selected periods, fireworks burning had stronger effects on the concentrations of K, Cu, Ba and Pb before and during the control period of the COVID-19 pandemic due to the Chinese Spring Festival.
(3) Nine types of sources contributing to the total elements in $PM_{2.5}$ were identified by PMF; they were fireworks burning, coal

combustion, vehicle emissions, dust, Zn smelter, Cr industry, Se industry, oil combustion, as well as iron and steel industry. The identification of fireworks burning made it possible to exclude its effects on the concentrations of elements from other sources. Compared with the concentrations before the control period, decrease during the control period was largest for the dust (89%), followed by the Cr industry (62%), coal combustion (62%), Zn smelter (58%), Se industry (43%), iron and steel industry (40%), while the concentrations from vehicle emissions and oil combustion increased by 115% and 53%, respectively.

(4) Air masses were clustered into five representative clusters: north northwest (26.5%), northwest (24.6% short and 16.7% long distance), northeast (23.5%) and southwest (8.7%). The strongest reductions of dust, coal combustion, Zn smelter, Cr industry, Se industry, and iron and steel industry occurred during the control period when the air masses came from the northwest. Compared to before the control period, they decreased by 92%, 100%, 95%, 77%, 64% and 87%, respectively. The lowest reductions for the Zn smelter, Se industry and iron and steel industry were noted for air mass transport from the northeast (Tangshan and Tianjin).

This study provided detailed variations of some primary $PM_{2.5}$ sources during the control period of the COVID-19 pandemic based on the measurement of elements. In a further study, combining other high-time resolution $PM_{2.5}$ chemical composition datasets (OC/EC, water-soluble-ions, etc.) could lead to a better understanding of the variations of the $PM_{2.5}$ sources (both primary and secondary sources).

CRediT authorship contribution statement

Yang Cui: Investigation, Formal analysis, Writing - original draft. **Dongsheng Ji:** Conceptualization, Investigation, Formal analysis, Writing - original draft. **Willy Maenhaut:** Conceptualization, Writing - review & editing. **Wenkang Gao:** Methodology, Writing - original draft. **Renjian Zhang:** Methodology, Writing - original draft. **Yuesi Wang:** Conceptualization, Writing - original draft.

Declaration of competing interest

The authors declare that they have no known competing financial interests or personal relationships that could have appeared to influence the work reported in this paper.

Acknowledgement

This work was supported by the National Key Research and Development Program of China (2017YFC0210000), the Chinese Academy of Sciences Key Technology Talent Program and the National Research Program for Key Issues in Air Pollution Control (DQGG0101 and DQGG0102). The authors like to thank all members of the LAPC/CERN in the IAP, CAS, for maintaining the instruments used in the current study.

Appendix A. Supplementary data

Supplementary data to this article can be found online at https://doi.org/10.1016/j.scitotenv.2020.140840.

References

Amato, F., Nava, S., Lucarelli, F., Querol, X., Alastuey, A., Baldasano, J., Pandolfi, M., 2010. A comprehensive assessment of PM emissions from paved roads: real-world emission factors and intense street cleaning trials. Sci. Total Environ. 408, 4309–4318.

Azhagurajan, A., Selvakumar, N., Thanulingam, T., 2011. Thermal and sensitivity analysis of nano aluminium powder for firework application. J. Therm. Anal. Calorim. 105, 259–267.

Baiduqianxi, 2020. https://qianxi.baidu.com.

Chang, Y., Huang, K., Xie, M., Deng, C., Zou, Z., Liu, S., Zhang, Y., 2018. First long-term and near real-time measurement of trace elements in China's urban atmosphere: temporal variability, source apportionment and precipitation effect. Atmos. Chem. Phys. 18, 11793–11812.

China News, 2020. https://news.china.com/focus/aqfg/13003576/20200316/37921943.html (in Chinese).

Cui, Y., Ji, D.S., Chen, H., Gao, M., Maenhaut, W., He, J., Wang, Y.S., 2019. Characteristics and sources of hourly trace elements in airborne fine particles in urban Beijing, China. J. Geophys. Res. Atmos. 11,595–11,613.

Dall'Osto, M., Querol, X., Amato, F., Karanasiou, A., Lucarelli, F., Nava, S., Calzolai, G., Chiari, M., 2013. Hourly elemental concentrations in $PM_{2.5}$ aerosols sampled simultaneously at urban background and road site during SAPUSS – diurnal variations and PMF receptor modelling. Atmos. Chem. Phys. 13, 4375–4392.

Duan, J., Tan, J., 2013. Atmospheric heavy metals and arsenic in China: situation, sources and control policies. Atmos. Environ. 74, 93–101.

Gao, J., Peng, X., Chen, G., Xu, J., Shi, G.L., Zhang, Y.C., Feng, Y.C., 2016. Insights into the chemical characterization and sources of $PM_{2.5}$ in Beijing at a 1-h time resolution. Sci. Total Environ. 542, 162–171.

Hebei News, 2020. http://gxt.hebei.gov.cn/hbgyhxxht/xwzx32/snxw40/667938/index.html (in Chinese).

Huang, K., Zhuang, G., Lin, Y., Wang, Q., Fu, J.S., Zhang, R., Li, J., Deng, C., Fu, Q., 2012. Impact of anthropogenic emission on air quality over a megacity–revealed from an intensive atmospheric campaign during the Chinese Spring Festival. Atmos. Chem. Phys. 12, 11631–11645.

Huang, X., Ding, A., Gao, J., Zheng, B., Zhou, D., Qi, X., Tang, R., Wang, J., Ren, C., Nie, W., Chi, X., Xu, Z., Chen, L., Li, Y., Che, F., Pang, N., Wang, H., Tong, D., Qin, W., Cheng, W., Liu, W., Fu, Q., Liu, B., Chai, F., Davaid, S.J., Zhang, Q., He, K., 2020. Enhanced secondary pollution offset reduction of primary emissions during COVID-19 lockdown in China. Natl. Sci. Rev., nwaa137 https://doi.org/10.1093/nsr/nwaa137.

Hubei COVID-19 Headquarter, 2020. Notice of COVID-19 epidemic from prevention and control headquarters in Hubei Province. http://www.wuhan.gov.cn/zwgk/tzgg/202004/t20200414_999364.shtml (in Chinese).

Khan, M., Latif, M.T., Saw, W., Amil, N., Nadzir, M.S.M., Sahani, M., Tahir, N., Chung, J., 2016. Fine particulate matter in the tropical environment: monsoonal effects, source apportionment, and health risk assessment. Atmos. Chem. Phys. 16, 597–617.

Kong, S.F., Li, L., Li, X.X., Yin, Y., Chen, K., Liu, D.T., Yuan, L., Zhang, Y.J., Shan, Y.P., Ji, Y.Q., 2015. The impacts of firework burning at the Chinese Spring Festival on air quality: insights of tracers, source evolution and aging processes. Atmos. Chem. Phys. 15, 2167–2184.

Li, Y., Chang, M., Ding, S., Wang, S., Ni, D., Hu, H., 2017. Monitoring and source apportionment of trace elements in $PM_{2.5}$: implications for local air quality management. J. Environ. Manag. 196, 16–25.

Li, L., Li, Q., Huang, L., Wang, Q., Zhu, A., Xu, J., Liu, Z., Li, H., Shi, L., Li, R., Azari, M., Wang, Y., Zhang, X., Liu, Z., Zhu, Y., Zhang, K., Xue, S., Chel Gee Ooi, M., Zhang, D., Chan, A., 2020. Air quality changes during the COVID-19 lockdown over the Yangtze River Delta Region: an insight into the impact of human activity pattern changes on air pollution variation. Sci. Total Environ. 732, 139282.

Lin, Y.C., Tsai, C.J., Wu, Y.C., Zhang, R., Chi, K.H., Huang, Y.T., Lin, S.H., Hsu, S.C., 2015. Characteristics of trace metals in traffic-derived particles in Hsuehshan Tunnel, Taiwan: size distribution, potential source, and fingerprinting metal ratio. Atmos. Chem. Phys. 15, 4117–4130.

Liu, J., Chen, Y., Chao, S., Cao, H., Zhang, A., Yang, Y., 2018. Emission control priority of $PM_{2.5}$-bound heavy metals in different seasons: a comprehensive analysis from health risk perspective. Sci. Total Environ. 644, 20–30.

Liu, J., Chen, Y., Chao, S., Cao, H., Zhang, A., 2019a. Levels and health risks of $PM_{2.5}$-bound toxic metals from firework/firecracker burning during festival periods in response to management strategies. Ecotoxicol. Environ. Saf. 171, 406–413.

Liu, Y., Zheng, M., Yu, M., Cai, X., Du, H., Li, J., Zhou, T., Yan, C., Wang, X., Shi, Z., Harrison, R.M., Zhang, Q., He, K., 2019b. High-time-resolution source apportionment of $PM_{2.5}$ in Beijing with multiple models. Atmos. Chem. Phys. 19, 6595–6609.

MEP, 2020. (Ministry of Environmental Protection of China). Five experts focused on the causes of air pollution in the Beijing-Tianjin-Hebei region and surrounding areasduring the control of Covid-19. http://www.mee.gov.cn/xxgk2018/xxgk/xxgk15/202002/t20200211_762584.html (in Chinese).

National Bureau of Statistics, 2017. China Statistical Yearbook 2017. China Statistics Press, Beijing (in Chinese).

Paatero, P., Eberly, S., Brown, S.G., Norris, G.A., 2014. Methods for estimating uncertainty in factor analytic solutions. Atmos. Meas. Tech. 7, 781–797.

Phillips-Smith, C., Jeong, C.-H., Healy, R.M., Dabek-Zlotorzynska, E., Celo, V., Brook, J.R., Evans, G., 2017. Sources of particulate matter components in the Athabasca oil sands region: investigation through a comparison of trace element measurement methodologies. Atmos. Chem. Phys. 17, 9435–9449.

Querol, X., Viana, M., Alastuey, A., Amato, F., Moreno, T., Castillo, S., Pey, J., De la Rosa, J., De La Campa, A.S., Artíñano, B., 2007. Source origin of trace elements in PM from regional background, urban and industrial sites of Spain. Atmos. Environ. 41, 7219–7231.

Richard, A., Gianini, M.F.D., Mohr, C., Furger, M., Bukowiecki, N., Minguillón, M.C., Lienemann, P., Flechsig, U., Appel, K., DeCarlo, P.F., Heringa, M.F., Chirico, R., Baltensperger, U., Prévôt, A.S.H., 2011. Source apportionment of size and time resolved trace elements and organic aerosols from an urban courtyard site in Switzerland. Atmos. Chem. Phys. 11, 8945–8963.

Tremper, A.H., Font, A., Priestman, M., Hamad, S.H., Chung, T.-C., Pribadi, A., Brown, R.J., Goddard, S.L., Grassineau, N., Petterson, K., Kelly, F.J., Green, D.C., 2018. Field and laboratory evaluation of a high time resolution x-ray fluorescence instrument for determining the elemental composition of ambient aerosols. Atmos. Meas. Tech. 11, 3541–3557.

Wang, Y., Zhang, X., Draxler, R.R., 2009. TrajStat: GIS-based software that uses various trajectory statistical analysis methods to identify potential sources from long-term air pollution measurement data. Environ. Model Softw. 24, 938–939.

Wang, Q., Qiao, L., Zhou, M., Zhu, S., Griffith, S., Li, L., Yu, J.Z., 2018. Source apportionment of $PM_{2.5}$ using hourly measurements of elemental tracers and major constituents in an urban environment: investigation of time-resolution influence. J. Geophys. Res. Atmos. 123, 5284–5300.

Wang, Q., Liu, S., Li, N., Dai, W., Wu, Y., Tian, J., Zhou, Y., Wang, M., Ho, S.S.H., Chen, Y., Zhang, R., Zhao, S., Zhu, C., Han, Y., Tie, X., Cao, J., 2019. Impacts of short-term mitigation measures on $PM_{2.5}$ and radiative effects: a case study at a regional background site near Beijing, China. Atmos. Chem. Phys. 19, 1881–1899.

Wang, P., Chen, K., Zhu, S., Wang, P., Zhang, H., 2020a. Severe air pollution events not avoided by reduced anthropogenic activities during COVID-19 outbreak. Resour. Conserv. Recycl. 158, 104814.

Wang, Y., Yuan, Y., Wang, Q., Liu, C., Zhi, Q., Cao, J., 2020b. Changes in air quality related to the control of coronavirus in China: implications for traffic and industrial emissions. Sci. Total Environ. 731, 139133.

WHO, 2020. https://covid19.who.int/.

Xu, K., Cui, K., Young, L.-H., Hsieh, Y.-K., Wang, Y.-F., Zhang, J., Wan, S., 2020. Impact of the COVID-19 event on air quality in Central China. Aerosol Air Qual. Res. 20, 915–929.

Zhang, J., Yang, L., Chen, J., Mellouki, A., Jiang, P., Gao, Y., Li, Y., Yang, Y., Wang, W., 2017. Influence of fireworks displays on the chemical characteristics of $PM_{2.5}$ in rural and suburban areas in Central and East China. Sci. Total Environ. 578, 476–484.

Zhang, R., Zhang, Y., Lin, H., Feng, X., Fu, T.-M., Wang, Y., 2020. NOx emission reduction and recovery during COVID-19 in East China. Atmosphere 11, 433.

Zhao, S., Hu, B., Gao, W., Li, L., Huang, W., Wang, L., Yang, Y., Liu, J., Li, J., Ji, D., Zhang, R., Zhang, Y., Wang, Y., 2020. Effect of the "coal to gas" project on atmospheric NOx during the heating period at a suburban site between Beijing and Tianjin. Atmos. Res. 241, 104977.

Zheng, H., Kong, S., Chen, N., Yan, Y., Liu, D., Zhu, B., Xu, K., Cao, W., Ding, Q., Lan, B., Zhang, Z., Zheng, M., Fan, Z., Cheng, Y., Zheng, S., Yao, L., Bai, Y., Zhao, T., Qi, S., 2020. Significant changes in the chemical compositions and sources of $PM_{2.5}$ in Wuhan since the city lockdown as Covid-19. Sci. Total Environ. 739, 140000.

Zhu, C., Tian, H., Hao, Y., Gao, J., Hao, J., Wang, Y., Hua, S., Wang, K., Liu, H., 2018. A high-resolution emission inventory of anthropogenic trace elements in Beijing-Tianjin-Hebei (BTH) region of China. Atmos. Environ. 191, 452–462.

Zíková, N., Wang, Y., Yang, F., Li, X., Tian, M., Hopke, P.K., 2016. On the source contribution to Beijing $PM_{2.5}$ concentrations. Atmos. Environ. 134, 84–95.